

High-frequency multilayer diffraction Si-gratings with a low blaze angle — fabrication

© D.V. Mokhov,¹ T.N. Berezovskaya,¹ E.V. Pirogov,¹ K.Yu. Shubina,¹ N.D. Prasolov,² M.V. Zorina,³ S.A. Garakhin,³ R.S. Pleshkov,³ N.I. Chkhalo,³ A.S. Dashkov,^{1,4} N.A. Kostromin,^{1,4} L.I. Goray,^{1,4,5,6} A.D. Bouravlev^{2,4,5,6}

¹Alferov University,
194021 St. Petersburg, Russia

²Ioffe Institute,
194021 St. Petersburg, Russia

³Institute for Physics of Microstructures RAS,
603087 Afonino, Kstovsky District, Nizhny Novgorod Oblast, Russia

⁴St. Petersburg Electrotechnical University „LETI“
197022 St. Petersburg, Russia

⁵Institute for Analytical Instrumentation RAS,
198095 St. Petersburg, Russia

⁶University under the IPA EurAsEC,
199226 St. Petersburg, Russia
e-mail: dm_mokhov@rambler.ru

Received April 17, 2024

Revised April 17, 2024

Accepted April 17, 2024

High-frequency X-ray diffraction gratings with a groove density of 2500 mm^{-1} and a low blaze angle were fabricated on Si(111)1.8° wafers using electron beam lithography and wet anisotropic etching. A multilayer Mo/Be coating consisting of 40 bilayers for a wavelength of 11.3 nm was deposited by magnetron sputtering. The groove profile during the fabrication of the gratings was monitored using atomic force microscopy and scanning electron microscopy. The averaged and random groove profiles and high- and mid-frequency roughness values of the best diffraction gratings obtained with atomic force microscopy will be used for subsequent simulation of the diffraction efficiency using the PCGrate™ code.

Keywords: Blazed diffraction Si-grating, low blaze angle, multilayer Mo/Be coating, electron beam lithography, wet anisotropic etching, magnetron sputtering, reflective facet roughness, atomic force microscopy, scanning electron microscopy, extreme UV.

DOI: 10.61011/TP.2024.07.58809.120-24

Introduction

Reflecting X-ray diffraction gratings with triangular groove profile („blazed“) are used for the inelastic resonance X-ray scattering spectroscopy, projection lithography in the extreme ultraviolet range (EUV) and beyond it, space mission instruments, X-ray free-electron laser end-stations and fourth-generation synchrotron radiation sources. The resonant inelastic X-ray scattering method requires diffraction gratings with extremely high resolution $\sim 10^5 - 10^6$ and maximum diffraction efficiency [1]. There are two main methods for achieving ultrahigh X-ray spectral resolution: use high-order diffraction of the blazed grating with a medium groove density or use first-order diffraction of the grating with high and ultrahigh groove density. It is known that gratings with a low or medium groove density and a small blaze angle α (reflecting facet angle) are required in the X-ray range to achieve high reflectances of gratings with one-layer coating and reduce the power density below the critical damage threshold [2,3].

High-frequency multilayer low blaze angle gratings (HMLBG) demonstrate good results in the EUV and soft X-ray (SXR) ranges. Mo₂C/C [4], Mo/Si [5–8], Sc/Si [9], W/B₄C [10], Al/Mo/SiC [11], Cr/C [12], etc., are used as multilayer reflective coating materials. Blazed gratings with multilayer coating are the most promising for the EUV and SXR ranges because they potentially concentrate almost all diffracted energy in the order of interest, however, their fabrication is more difficult because they require very high quality of a „sawtooth“ grating [7].

The study in Ref. [5] reports about fabrication by the ion etching method of a 2400 mm^{-1} grating with $\alpha = 1.9^\circ$ and Mo/Si multilayer coating that has the absolute (relative to the incident beam intensity) second negative order diffraction efficiency $\eta(-2) = 36.2\%$ with the incident angle $\theta = 10^\circ$ and wavelength $\lambda = 13.62\text{ nm}$. The study in Ref. [4] reports about 3000 mm^{-1} holographic grating with $\alpha = 2.78^\circ$ and Mo₂C/C multilayer coating fabricated using the ion-etching method with the measured $\eta(-2)$ equal to 29.9% at $\theta = 5.6^\circ$ and $\lambda = 15.79\text{ nm}$, and the

relative (relative to the reflectance of a multilayer witness mirror) efficiency of 53.0%. The grating with a groove density of 5000 mm^{-1} , $\alpha = 6^\circ$ and $(\text{Mo/Si}) \times 30$ coating demonstrated $\eta(-3) = 37.6\%$ at $\lambda = 13.6\text{ nm}$ [13]. $\eta(-8) = 40\%$ of unpolarized radiation was obtained for $\lambda = 13.6\text{ nm}$ and $\theta = 70.5^\circ$ for a 500 mm^{-1} grating with $\alpha = 3.9^\circ$ and $(\text{Mo/Si}) \times 5$ coating, which is a record for a medium-frequency grating operating in a high order [8].

The study in Ref. [14] describes a 100 mm^{-1} grating with the ultra-low blaze angle $\alpha = 0.04^\circ$ and Mo/Si multilayer coating that demonstrates a record-breaking EUV diffraction efficiency $\eta(-1) = 58\%$. The authors have developed a quite sophisticated process to reduce the blaze angle from 4° to 0.04° for the Si grating fabricated by anisotropic wet etching: first, smoothing the surface with a polymer layer, and then removal of the polymer and underlying Si by plasma etching. The study in Ref. [15] demonstrates that the master-grating blaze angle is reduced by a factor of 5 when fabricating a 200 mm^{-1} grating with $\alpha = 0.2^\circ$. However, the multistage double copying method and nonuniform plasma etching with reduction of the blaze angle result in a degradation of the reflecting facet surface; the resist surface roughness often moves to the facet surface that, in addition, inherits high degree of curvature from the master-grating. Moreover, it is difficult to implement these processes for high-frequency gratings.

Since the blazed gratings are the best candidates for the achievement of high efficiency in any diffraction order, it is extremely important to obtain a near-ideal triangular asymmetric groove profile with the smooth and flat surface of reflecting facets. We concentrated our efforts in our studies on obtaining highly efficient gratings with an ideal triangular asymmetric profile and defined some minimum requirements (criteria) for evaluation of the grating quality, which we apply for the development and optimization of fabrication processes. It is obvious that the efficiency (reflectivity) of a blazed grating is defined by the reflecting surface area and quality, whereas the reflecting surface area is defined by the length of reflecting facets. The reflecting facet length l should satisfy $l \geq 0.75d$ (d is the grating period) after removal of Si nubs in smoothing and polishing etchant. The groove profile should remain asymmetric after smoothing and polishing etching (the antiblaze angle γ should not be reduced considerably during etching) and we use an asymmetry factor calculated as a ratio between the antiblaze angle and blaze angle ($k = \gamma/\alpha$), which should be $k \geq 5$, as an asymmetry criterium. However, the reflection of radiation into the order of interest involves a part of the reflecting facet (so-called effective length) not shaded by Si nubs both for the incident and reflected (diffracted) radiation as well as it has the same effective angle throughout its length. Figure 1 shows the negative impact of the remaining Si nubs (Figure 1, *a*) that reduce the effective facet length. The geometry defines a part of the illuminated facet area (a part of the facet may be self-shaded (Figure 1, *b*)), whereas the effective blaze angle may

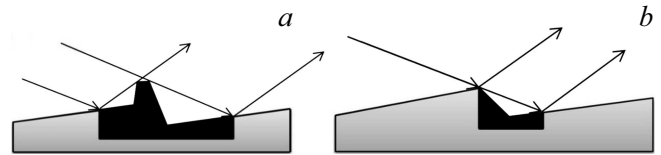


Figure 1. Schematic image of the radiation reflected by the reflecting facet of the blazed grating: *a* — with remaining Si nubs; *b* — without Si nubs.

be estimated as a medium slope of the unshaded part of the reflecting facet.

The quality of the reflecting surface depends on the surface flatness (curvature effect) and smoothness (roughness effect) of the reflecting facet. The authors of Ref. [3] believe that the curvature effect of the reflecting facet on the grating efficiency should be considered for particular groove profiles and diffraction geometry that defines a part of the illuminated facet area. They note that the curvature effect may be significant if the facet surface out-of-flatness is comparable with the groove depth. The researchers in Ref. [7] highlight a problem of significant groove surface curvature in gratings with a period of $4 - 10\ \mu\text{m}$ due to uneven distribution of density of atomic steps over the grating facet. To avoid this problem, it is possible to fabricate high-frequency gratings with mean blaze angles of $1^\circ - 10^\circ$ and a period of $100 - 500\text{ nm}$, as their efficiency is not affected so much by the groove curvature. It should be noted that the reflecting facet curvature of the grating not only reduces the effective length of the reflecting facet, but also affects the maximum achievable working order number at which the maximum diffraction efficiency remains unchanged as we found in Ref. [16].

Surface smoothness depends on the irregularity sizes that are characterized by random roughness. We agree with the researchers in Ref. [7] that the grating fabrication process should ensure both precise control of the groove profile and low groove surface roughness. The reflecting facet surface of the blazed grating has high-frequency and medium-frequency (usually exhibited as ripples) roughness on which incident radiation scattering occurs. Our studies of the effect of random roughness of the reflecting facet on the diffraction efficiency in Ref. [17] found that an additional parameter was required to determine accurately the roughness statistics of the given surface and to use the data properly for simulation of the diffraction efficiency of gratings with a realistic groove profile and taking into account the random roughness. Therefore, we use not only the high-frequency roughness component measured using the atomicforce microscopy (AFM) in the $1 \times 1\ \mu\text{m}$ field for describing the surface roughness in our practical work, but also the medium-frequency component measured by 1D scanning of the reflecting facet surface at a length of $20\ \mu\text{m}$ along the groove. The requirements for the root mean square (Rms) high-frequency roughness $\text{Rms} \leq 0.50\text{ nm}$ ($1 \times 1\ \mu\text{m}$) and medium-frequency rough-

ness $R_{ms} \leq 1.5 \text{ nm}$ (length $20 \mu\text{m}$) are the criteria of the adequate smoothness of the reflecting surface.

We successfully improved the reflecting facet parameters (maximum length, minimum curvature and allowable roughness) by optimizing the grating fabrication process and also the parameters of the whole grating (absence of the Si nubs, triangular profile asymmetry, parameter uniformity across the grating aperture, absence of defects on the reflecting facet surface) that collectively affected the grating diffraction efficiency.

The results of the optimization of the fabrication technique of HMLBG with $\alpha \sim 1^\circ - 2^\circ$ and acceptable parameters are provided herein. These results were achieved using the grating acceptance criteria and the previously developed technique of fabrication of medium- and high-frequency gratings with blaze angles of $2^\circ - 4^\circ$ by anisotropic wet etching of silicon. A unique reflective multilayer Mo/Be coating was applied to the Si master-grating using the magnetron sputtering method after its fabrication with the acceptable parameters.

1. Fabrication of gratings

HMLBG with the constant of $d \approx 400 \text{ nm}$ are made using the previously developed technique of fabrication of medium-frequency gratings with $\alpha \sim 4^\circ$ [18].

Silicon oxide or silicon nitride masks made by reactive ion etching are most often used as a protective etching mask. One of the disadvantages of these masks is that the mask material dissolves in the BHF used to remove oxide from the silicon surface before KOH etching, therefore very thick layers should be applied and long-term repeated treatment in BHF should be avoided, which is not convenient because the same sample often has to be etched in KOH several times to achieve the desired angle. Another disadvantage of these masks is the silicon surface damage during the deposition of the materials and also during reactive ion etching of the materials, which is probably associated with formation of nanowells during subsequent removal of Si nubs in piranha solution (or RCA-1) oxidation/HF etching cycles that are generally used by researchers [19].

We tried silicon nitride and chromium as the etching mask material when developing the etching technique. The silicon oxide was not chosen for the study because it dissolved not only in BHF, but also in KOH, therefore a thick layer should be applied. We applied the layer of stoichiometric Si_3N_4 using the low-temperature plasma enhanced chemical vapor deposition (PECVD). The Si_3N_4 mask was obtained by BHF wet etching or inductively coupled plasma (ICP) etching of silicon nitride through an organic photoresist mask. No defects were found after etching when the open silicon surface on nitride mask was examined by the scanning electron microscopy (SEM) method. However, ripple-form defects were found on the reflecting facet surfaces after KOH etching of a sample with the Si_3N_4 -mask produced by wet etching and ripple-form defects and deep wells were

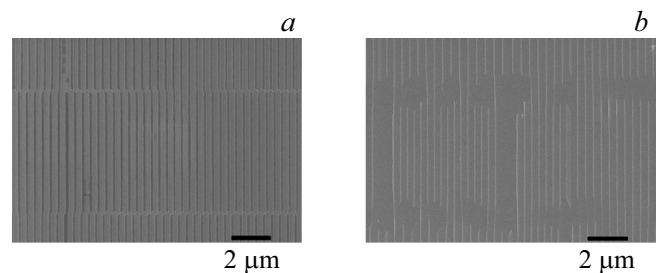


Figure 2. SEM plan-view images of Sv-4-2 grating surface: *a* — EBL mask; *b* — after KOH etching and removal of Si nubs.

found on a sample with the Si_3N_4 -mask formed by the ICP etching. These defects can be probably attributed to the silicon surface damage during the silicon nitride deposition.

As for chromium, we tested two Cr mask formation methods: cerium wet etching through an organic photoresist mask [18] applicable only to gratings with the constant $\geq 2 \mu\text{m}$ and metal lift-off technique [20]. We chose the chromium fabricated by the metal lift-off technique because this is a multipurpose process (suitable for any grating), it is sufficient to apply a $\sim 20 \text{ nm}$ layer for protection, chromium is resistant to HF, BHF and KOH solutions, it does not damage the silicon surface during sputtering and can be easily removed.

For Si gratings with different constants and different blaze angles it is important to choose the optimal Cr strip width on the protective mask (the angle defines etching depth and, therefore, time): too narrow strips will not provide protection during anisotropic alkaline etching, and too wide ones will lead to the wide Si Nubs formation and, thus, a decrease in the reflecting facet length. The gratings were fabricated using boron-doped Si(111) wafers with a misorientation angle of 1.8° , resistivity of $0.015 \Omega \cdot \text{cm}$, $\varnothing 100 \text{ mm}$ and thickness of 1.5 mm . To select the optimal strip width of the protective mask, a $15 \times 15 \text{ mm}$ Cr mask was fabricated on the surface of three fragments with size equal to 1/4 of the Si(111) wafer by the metal lift-off technique using a single-layer electron-beam lithography mask (EBL mask) with different exposure. The EBL mask was recorded in the organic resist layer by electron beam with $6.3 \times 6.3 \mu\text{m}$ exposure fields in the lithography system. The resistive mask was developed in MIK:IPA (methylisobutyl ketone:isopropyl alcohol = 1:3) mixture using an automatic electron resist developing system. The quality of the EBL mask defines the quality of the future grating. Poor exposure field stitching areas may occur during EBL mask recording that are later developed as areas with offset pattern, with pattern discontinuities and with a different pattern period (Figure 2). Stitching areas negatively affect the grating resolution and reduce its efficiency. Deep etching is observed in these areas: Figure 3 shows the AFM profiles obtained by measuring medium-frequency roughness along

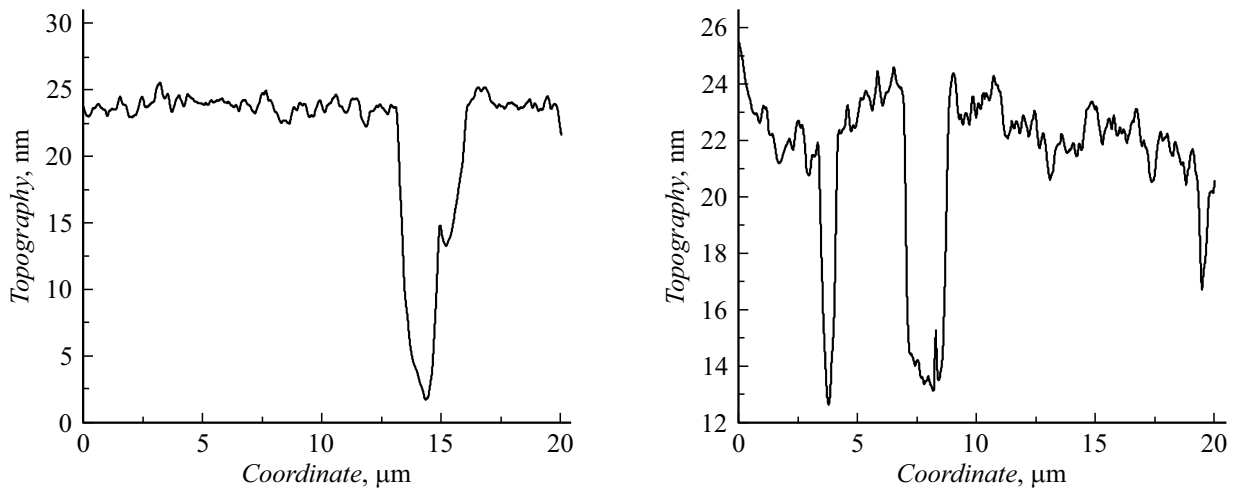


Figure 3. 1D scan of Sv-4-2 grating surface along the groove on the length of 20 μm .

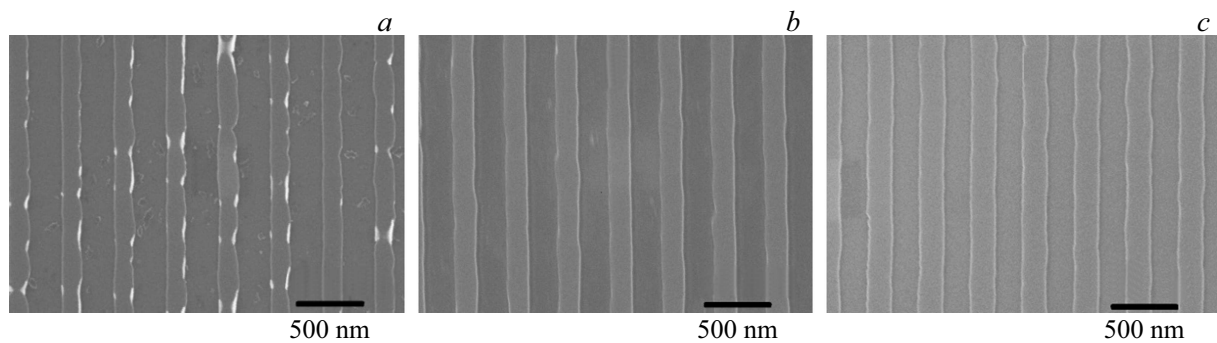


Figure 4. SEM images of Cr mask with exposure: *a* — 500, *b* — 600, *c* — 700 c.u.

the groove surface with scan length of 20 μm in two areas.

The Cr mask was obtained by vacuum deposition of a 20 nm chromium layer to the samples with developed EBL mask and lifting-off in dimethylformamide. Figure 4 shows the SEM plan view images of the obtained Cr mask with the strip widths of 126, 169 and 183 nm and an exposure of 500, 600 and 700 c.u., respectively.

Adhesion of the Cr mask to Si for all samples was good: Cr mask did not separated in any sample after anisotropic etching in 20% KOH solution. We chose an exposure of 600 c.u., because the sample had the lowest width of Si nubs after KOH etching. However, discontinuities and pattern strip width narrowing were observed in some field stitching areas due to the lack of exposure of these ones during field stitching, and, therefore, an optimization of the recording mode was required. To optimize the EBL mask recording mode, which provides accurate stitching of the exposure fields and prevents grating period failure, as well as to check the reproducibility of the mask parameters and the wafer etching homogeneity, a single-layer EBL mask was formed with an exposure of 600 c.u. on three 15 \times 15 mm squares. Then, the Cr mask was fabricated and anisotropic KOH

etching was performed. After anisotropic KOH etching, the protective Cr mask was removed with cerium etchant.

During KOH etching, on the ridge of the triangular profile Si nubs are formed as a result of side etching of Si under the protective mask (Figure 5, *a* on top). The Si nub removal and reflecting facet surface polishing method that we developed for medium-frequency gratings [20] was optimized for high-frequency gratings and applied for HMLBG: the Si nubs (26 nm height, 78 nm width) on the grating profile were removed by wet etching in a smoothing and polishing etchant. Smoothing and polishing etching was controlled by the width of Si nubs on the SEM plan view images using the Zeiss Supra 25 microscope (Figure 5, bottom) and by profile measurements using an atomic-force microscope (Figure 5, top). After removal of Si nubs, the reflecting facet length of Sv-4-3 grating increased by 53% and met the minimum requirements for an X-ray grating.

2. Characterization of the groove profile and Mo/Be coating deposition

The perfection of the grating groove profile is one of the most important parameters of blazed gratings, therefore

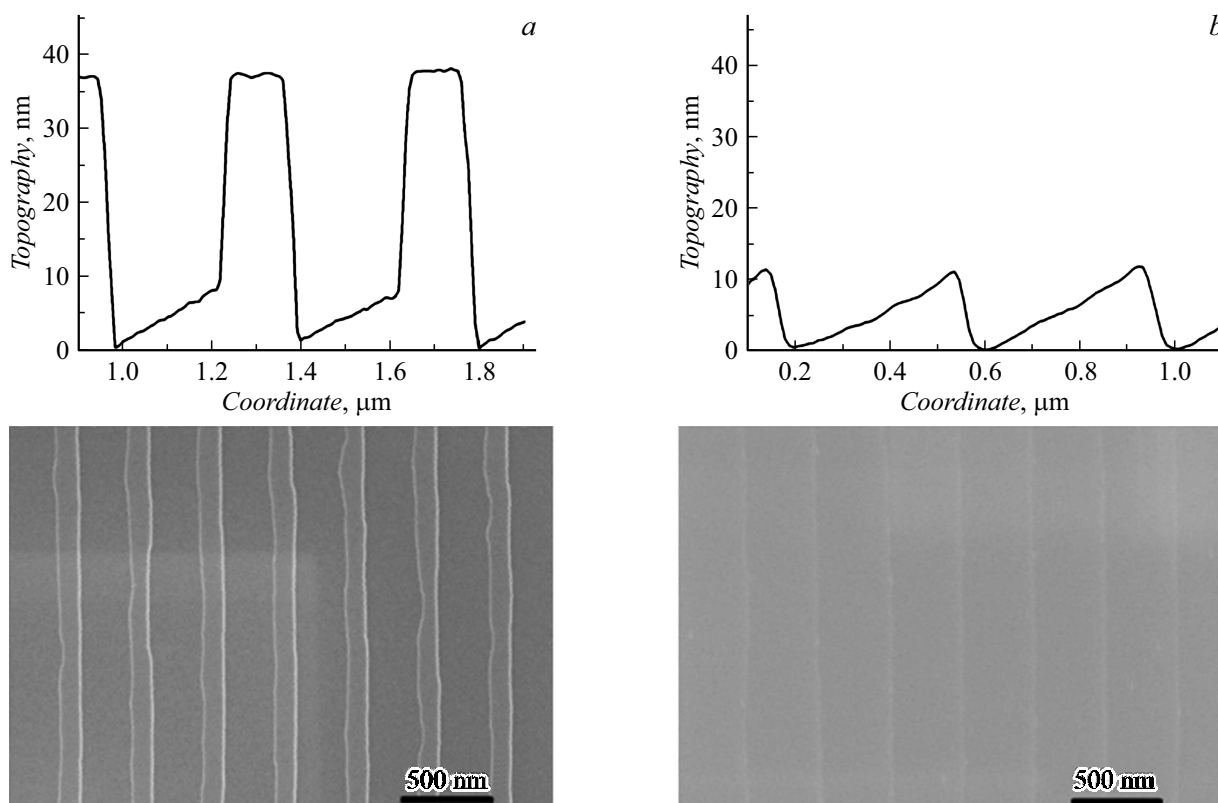


Figure 5. AFM profiles and SEM images 100 m.u. of Sv-4-3 grating surface: *a* — before removal of Si Nubs; *b* — Si Nubs are removed.

a thorough characterization is required for controlling the parameter variation during fabrication, obtaining data for grating quality assessment and efficiency prediction, for the analysis of parameter uniformity across the grating aperture, etc. The grating characterization uses absolute and relative efficiency, resolution and design parameters on which the efficiency depends. The last ones include design parameters of the whole grating and of the groove. The grating design parameters are: grating shape and dimensions (width×length×thickness); grating material; reflective coating composition and thickness. Groove design parameters are: grating period (law of variation of period for gratings with variable spacing and groove curvature for curvilinear gratings), groove depth, length, blaze angle, curvature and random roughness of the reflecting facet, antireflection facet angle, groove profile shape, reflecting facet and grating surface appearance. We developed a method to determine the groove parameters of a diffraction grating. The groove profiles are scanned on a length of 5–10 grating periods depending on the groove density: on a length of 10 periods — for gratings with a period from 0.2 to 4 μm, on a length of 5 periods — for gratings with a period from 4 to 10 μm. The profiles are scanned in several areas depending on the grating size and purpose of measurement. For example, the profile measurement to evaluate parameter distribution uniformity over the grating area Ø 76.2 mm is performed in seven regions.

The smoothness of the reflecting surface of the working facet was characterized using the additional medium-frequency roughness measured on a length of 20 μm along the groove (1D scan of the surface along the groove). Figure 6 shows the results of AFM 2D scanning (Figure 6, *a*) and 1D scanning along the groove (Figure 6, *b*) of Sv-4-3 grating surface before sputtering the reflective coating.

Averaged parameters of three fabricated gratings before reflective coating deposition are listed in the table. The parameters of the reflecting facet (length l and roughness Rms) of Sv-4-2 grating did not meet the minimum requirements for X-ray grating as shown in the Table: $l \geq 0.75d$, $Rms \leq 0.5 \text{ nm}$ ($1 \times 1 \mu\text{m}$). The image of Sv-4-3 grating with better parameters before deposition of reflective coating is shown in Figure 7.

Since Sv-4-2 grating had significant stitching error (Figures 2 and 3), and high-frequency roughness and reflecting facet length did not meet the minimum requirements for X-ray gratings, no reflecting coating was deposited to it, and a transverse cleavage was made for SEM examination of the profile and surface (Figure 8). Figure 8, *a* shows that the grating profile is almost ideal triangular, asymmetric, and Figure 8, *c* shows etching marks due to stitching during the EBL mask recording.

A reflective coating is deposited to the grating to increase the reflectance. The composition and thickness of the coating depend on the diffraction grating application with respect to spectral range, operation scheme and use

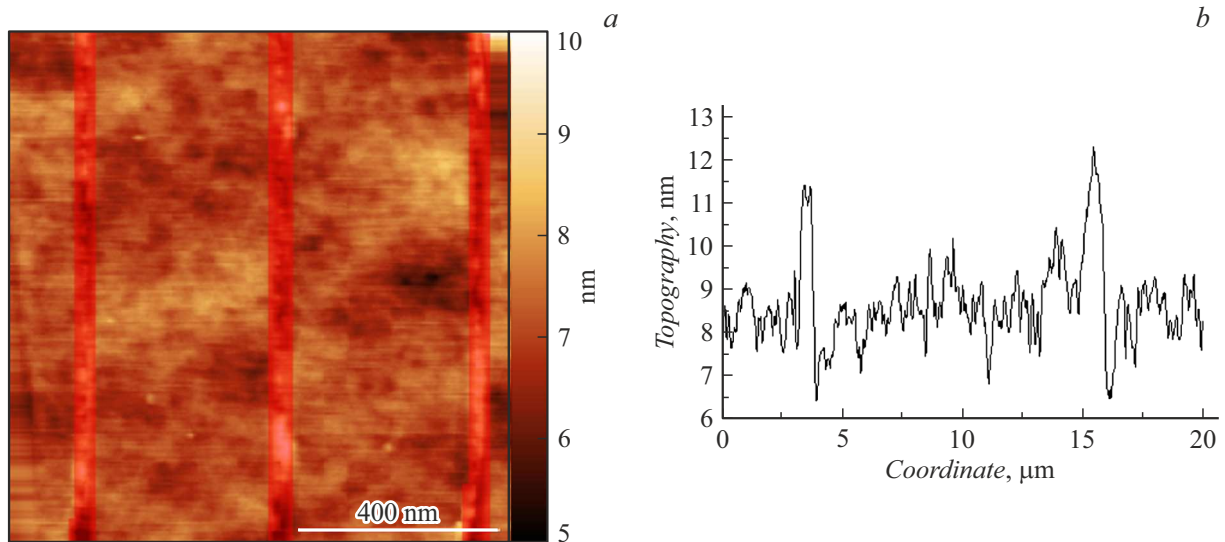


Figure 6. AFM topography of Sv-4-3 grating without coating: *a* — Rms=0.37 nm ($1 \times 1 \mu\text{m}$); *b* — Rms=0.60 nm (on the length of $20 \mu\text{m}$).

Grating parameters before reflective coating deposition

| Grating | Groove depth, nm | Length of reflective edge, nm | Blaze angle, ° | Roughness, Rms, nm | |
|---------|------------------|-------------------------------|----------------|------------------------------|----------------------|
| | | | | ($1 \times 1 \mu\text{m}$) | ($20 \mu\text{m}$) |
| Sv-4-1 | 11 | 345 | 1.8 | 0.45 | 0.69 |
| Sv-4-2 | 9 | 292 | 1.8 | 0.80 | 0.71 |
| Sv-4-3 | 11 | 356 | 1.8 | 0.39 | 0.70 |

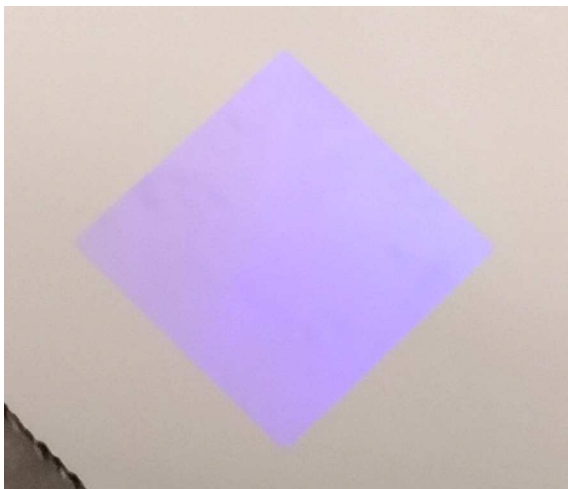


Figure 7. Image of Sv-4-3 grating ($15 \times 15 \text{ mm}$).

conditions. The gratings are designed to be used in classical scheme (in a plane perpendicular to grooves) with the near-normal incidence ($\theta = 0^\circ - 8^\circ$) of $\lambda = 11.3 \text{ nm}$ EUV radiation. A reflective multilayer Mo/Be coating with the number of periods $N = 40$, period $\sim 5.7 \text{ nm}$ and layer thickness of 2.25 nm (Mo) and 3.45 nm (Be) was applied

to Sv-4-1 and Sv-4-3 gratings by the magnetron sputtering method. A Si wafer fragment was placed near the grating for coating deposition to be used as a reflecting coating witness to measure layer thickness, interlayer roughness (diffuseness), period and reflectance of the multilayer Mo/Be coating. The reflectance measured for the multilayer coating (Mo/Be) $\times 40$ witness was equal to $\sim 60\%$ due to the interface diffusivity (and lower material density), which was 12% lower than the maximum reflectance for the chosen multilayer coating at $N = 40$.

The triangular groove profile and random roughness varied insignificantly as follows from the comparison of the AFM scanning results for Sv-4-3 grating without reflective coating (Figure 6, *a*) and after sputtering of the reflective multilayer Mo/Be coating with a total thickness of $\sim 230 \text{ nm}$ (Figure 9): the blaze angle decreased from 1.78° to 1.69° (and the groove depth decreased from 11.0 to 9.2 nm), roughness Rms ($1 \times 1 \mu\text{m}$) increased from 0.39 nm to 0.46 nm .

Conclusion

Several blazed diffraction grating samples with $d \sim 400 \text{ nm}$, low $\alpha \approx 1.7^\circ$ and area equal to several square centimeters were fabricated using electron-beam

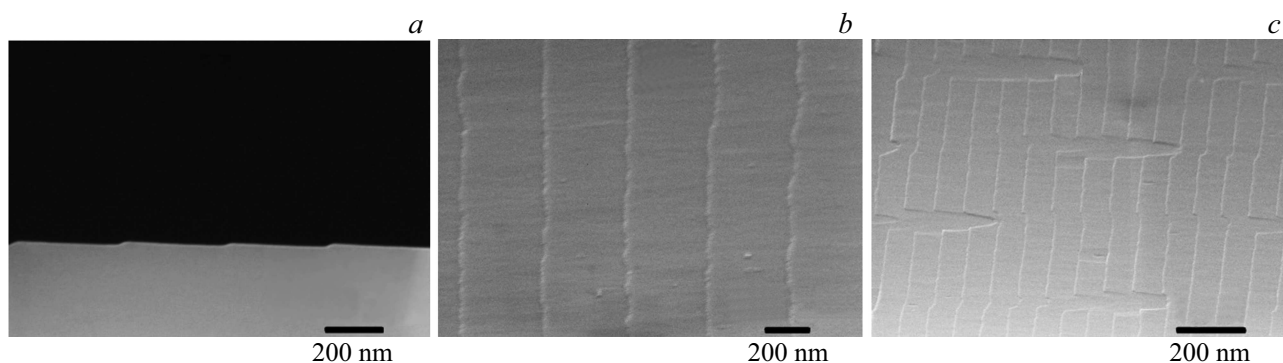


Figure 8. SEM images of Sv-4-2 grating: *a* — cross-section, *b* — isometry at 10° , *c* — isometry at 10° .

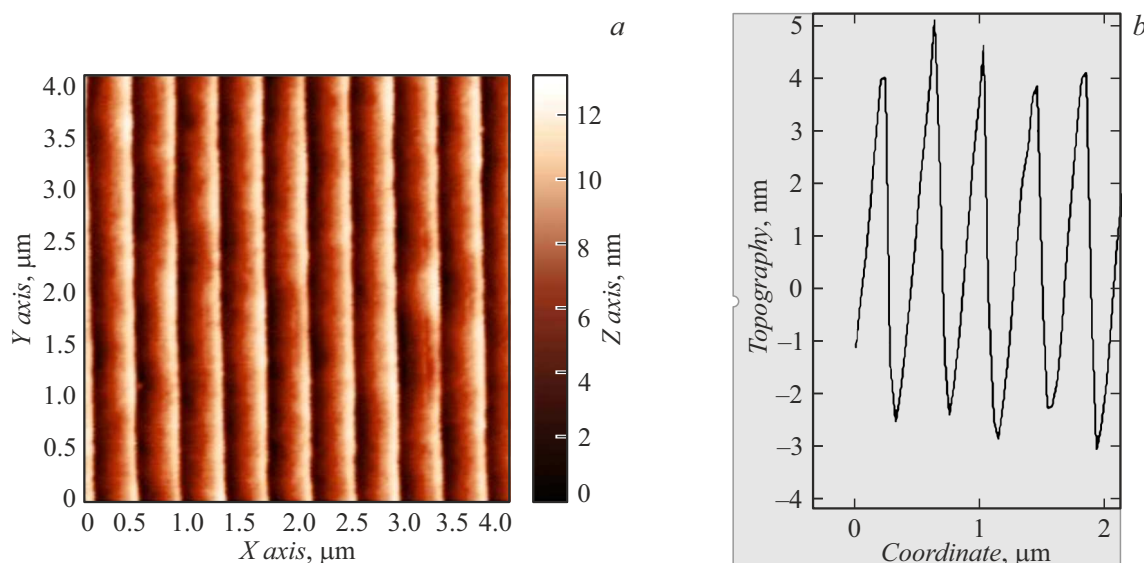


Figure 9. Sv-4-3 grating with Mo/Be coating: *a* — AFM topography; *b* — AFM profile.

lithography and only anisotropic wet etching of the Si(111) 1.8° wafers. The optimized fabrication process ensured the precise control of grating parameters and grating groove profile both with very short antireflection facets and atomically-smooth surface of the blazed facets.

The first Mo/Be HMLBG (Sv-4-3) was fabricated using magnetron sputtering and was qualified for application in the classical diffraction configuration with $\lambda = 11.3$ nm. The Si master-grating and original multilayer grating fabricated with deposition of 40 periods of the Mo/Be coating with a total thickness of ~ 230 nm have a near-ideal triangular asymmetric groove profile with the acceptable surface roughness of reflecting facets.

The fabricated HMLBG are designed for application in the classical optical scheme (in a plane perpendicular to grooves) with the near-normal incidence ($\theta = 0^\circ - 8^\circ$) of $\lambda = 11.3$ nm radiation. The absolute diffraction efficiency of gratings measured using the laboratory reflectometer with Czerny-Turner high-resolution spectrometer [21] and calculated by simulation in PCGrateTM v.6.7.1 [22] using

averaged AFM groove profiles and AFM distributions of random roughness was about 38% in -2 order [23].

We are planning to focus our future efforts on the optimization of the EBL mask recording modes to avoid (reduce) the stitching error and improve the uniformity of grating parameters across the area, and on the improvement of the multilayer Mo/Be coating deposition process to increase its reflectance to the value close to the theoretical limit.

Funding

The study performed by T.N. Berezovskaya, L.I. Goray, A.S. Dashkov, D.V. Mokhov, E.V. Pirogov and K.Yu.Shubina was supported by the Ministry of Education and Science of the Russian Federation (FSRM-2023-0006) in terms of experimental investigations. The study performed by L.I. Goray, A.S. Dashkov and N.A. Kostromin was supported by the Russian Science Foundation (№ 23-29-00216) in terms of theoretical research.

Conflict of interest

The authors declare that they have no conflict of interest.

References

- [1] L.J.P. Ament, M. van Veenendaal, T. Devereaux, J.P. Hill, J. van den Brink. *Rev. Mod. Phys.*, **83**, 705 (2011). DOI: 10.1103/RevModPhys.83.705
- [2] L. Goray, W. Jark, D. Eichert. *J. Synchrotron Radiation*, **25** (6), 1683 (2018). DOI: 10.1107/S1600577518012419
- [3] D.L. Voronov, P. Lum, P. Naulleau, E.M. Gullikson, A.V. Fedorov, H.A. Padmore. *Appl. Phys. Lett.*, **109**, 043112 (2016). DOI: 10.1063/1.4960203
- [4] M.P. Kowalski, R.G. Cruddace, K.F. Heidemann, R. Lenke, H. Kierey, T.W. Barbee, W.R. Hunter. *Opt. Lett.*, **29** (24), 2914 (2004).
- [5] H. Lin, L. Zhang, L. Li, Ch. Jin, H. Zhou, T. Huo. *Opt. Lett.*, **33** (5), 485 (2008). DOI: 10.1364/ol.33.000485
- [6] F. Salmassi, P.P. Naulleau, E.M. Gullikson, D.L. Olynick, J.A. Liddle. *J. Vacuum Sci. Technol. A Vacuum Surfaces and Films*, **24** (4), 1136 (2006). DOI: 10.1116/1.2212435
- [7] D.L. Voronov, E.H. Anderson, R. Cambie, F. Salmassi, E.M. Gullikson, V.V. Yashchuk, H.A. Padmore, M. Ahn, C.-H. Chang, R.K. Heilmann, M.L. Schattenburg. *Proc. SPIE*, **7448**, 74480J (2009). DOI: 10.1117/12.826921
- [8] L.I. Goray, T.N. Berezovskaya, D.V. Mokhov, V.A. Sharov, K.Yu. Shubina, E.V. Pirogov, A.S. Dashkov, A.V. Nashchekin, M.V. Zorina, M.M. Barysheva, S.A. Garakhin, S.Yu. Zuev, N.I. Chkhalo. *Bull. Lebedev Phys. Institute*, **50** (2), S250 (2023). DOI: 10.3103/S1068335623140063
- [9] D.L. Voronov, R. Cambie, E.M. Gullikson, V.V. Yashchuk, H.A. Padmore, Yu.P. Pershin, A.G. Ponomarenko, V.V. Kondratenko. *Proc. SPIE*, 7077, 707708-1 (2008). DOI: 10.1117/12.795377
- [10] D.L. Voronov, T. Warwick, H.A. Padmore. *Opt. Lett.*, **39** (21), 6134 (2014). DOI: 10.1364/OL.39.006134
- [11] A.H.K. Mahmoud, S. de Rossi, E. Meltchakov, B. Capitano, M. Thomasset, M. Vallet, E. Heripre, F. Delmotte. *Opt. Express*, **30** (21), 38319 (2022). DOI: 10.1364/OE.468568
- [12] A. Sokolov, Q. Huang, F. Senf, J. Feng, S. Lemke, S. Alimov, J. Knedel, T. Zeschke, O. Kutz, T. Seliger, G. Gwalt, F. Schäfers, F. Siewert, I.V. Kozhevnikov, R. Qi, Z. Zhang, W. Li, Z. Wang. *Opt. Express*, **27** (12), 16833 (2019). DOI: 10.1364/OE.27.016833
- [13] D.L. Voronov, M. Ahn, E.H. Anderson, R. Cambie, Ch.-H. Chang, L.I. Goray, E.M. Gullikson, R.K. Heilmann, F. Salmassi, M.L. Schattenburg, T. Warwick, V.V. Yashchuk, H.A. Padmore. *Proc. SPIE*, **7802**, 780207 (2010). DOI: 10.1117/12.861287
- [14] S. Park, D.L. Voronov, E.M. Gullikson, F. Salmassi, H.A. Padmore. *Proc. SPIE*, **11837**, 118370I (2021). DOI: 10.1117/12.2596269
- [15] D.L. Voronov, S. Park, E.M. Gullikson, F. Salmassi, H.A. Padmore. *Opt. Express*, **31** (16), 26724 (2023). DOI: 10.1364/OE.495374
- [16] L.I. Goray, T.N. Berezovskaya, D.V. Mokhov, V.A. Sharov, K.Yu. Shubina, E.V. Pirogov, A.S. Dashkov. *J. Surf. Investigation: X-ray, Synchrotron and Neutron Techniques*, **17** (1), S104 (2023). DOI: 10.1134/S1027451023070145
- [17] L.I. Goray, V.A. Sharov, D.V. Mokhov, T.N. Berezovskaya, K.Yu. Shubina, E.V. Pirogov, A.S. Dashkov, A.D. Bouravlev. *Tech. Phys.*, **68** (7), 797 (2023). DOI: 10.61011/TP.2023.07.56619.66-23
- [18] L.I. Goray, T.N. Berezovskaya, D.V. Mokhov, V.A. Sharov, K.Yu. Shubina, E.V. Pirogov, A.S. Dashkov. *Tech. Phys.*, **91** (10), 1531 (2021). DOI: 10.61011/TP.2024.07.58809.120-24
- [19] D.L. Voronov, E.H. Anderson, R. Cambie, F. Salmassi, E.M. Gullikson, V.V. Yashchuk, H.A. Padmore, M. Ahn, C.-H. Chang, R.K. Heilmann, M.L. Schattenburg. *Proc. SPIE*, **7448**, 74480J (2009). DOI: 10.1117/12.826921
- [20] D.V. Mokhov, T.N. Berezovskaya, K.Yu. Shubina, E.V. Pirogov, A.V. Nashchekin, V.A. Sharov, L.I. Goray. *Tech. Phys.*, **92** (8), 1009 (2022). DOI: 10.61011/TP.2024.07.58809.120-24
- [21] S.A. Garakhin, N.I. Chkhalo, I.A. Kas'kov, A.Ya. Lopatin, I.V. Malyshev, A.N. Nechay, A.E. Pestov, V.N. Polkovnikov, N.N. Salashchenko, M.V. Svechnikov, N.N. Tsybin, I.G. Zabrodin, S.Yu. Zuev. *Rev. Sci. Instrum.*, **91** (6), 063103 (2020).
- [22] Electronic source. Available at: www.pcgrate.com
- [23] L.I. Goray, A.S. Dashkov, N.A. Kostromin, D.V. Mokhov, T.N. Berezovskaya, E.V. Pirogov, K.Yu. Shubina, V.A. Sharov, N.D. Prasolov, M.V. Zorina, S.A. Garakhin, R.S. Pleshkov, N.I. Chkhalo, A.D. Buravlev. *ZhTF*, **94** (7), 2024 (in Russian).

Translated by E.Ilinskaya